Supporting Information:

Persistent Inter-Excitonic Quantum Coherence in CdSe Quantum Dots

Justin R. Caram[1], Haibin Zheng[1], Peter D. Dahlberg[2], Brian S. Rolczynski[1], Graham B. Griffin[1], Andrew F. Fidler[1], Dmitriy S. Dolzhnikov[3], Dmitri V. Talapin[3], and Gregory S. Engel[1,a]

1. Department of Chemistry, The Institute for Biophysical Dynamics, and The James Franck Institute, The University of Chicago, Chicago, Illinois 60637, USA
2. Graduate Program in the Biophysical Sciences, The Institute for Biophysical Dynamics, and The James Franck Institute, The University of Chicago, Chicago, IL 60637
3. Department of Chemistry, and The James Franck Institute, The University of Chicago, Chicago, Illinois 60637, USA

a) To whom correspondence should be addressed. E-mail: gsengel@uchicago.edu

Synthesis of Quantum Dots

Large CdSe quantum dots were made using literature procedure.[1] 0.2 mmol of cadmium myristate, 0.2 mmol of selenium dioxide and 0.04 mmol of cadmium acetate were mixed in 12.6 mL of 1-octadecene. The solution was heated to 240 °C (heat rate ~20 °C/min) and stirred. Once the solution reached 230 °C ,0.2 mL of oleic acid was added to stabilize the growth of nanocrystals. Quantum dots were precipitated with ethanol and re-dispersed in toluene after an hour. Washing was repeated 2 times. We obtained transmission electron microscopy (TEM) images (FEI Tecnai F30 microscope) at 300 kV. To determine zinc blende crystallinity, powder X-ray diffraction was collected (Bruker D8 diffractometer). The TEM image and XRD pattern are shown in figure S1a and S1b , with an inset showing a size histogram of dot size. We also plot a histogram of sizes generated by examining the TEM image in the inset. In figure S2, we plot the absorption spectrum fit to Gaussians to estimate the position of the spectral features; our results are consistent with more monodisperse, well resolved preparations.

C-2DES Apparatus

Continuum two dimensional spectroscopy differs from other implementations of 2DES in two specfic ways. First, it utilizes continuum generation in argon to generate ultrabroadband "white" light, and utilizes that light for all four pulse interactions.[2] These pulses span 400 to 900 nm, from which a 180 nm region in the visible is selected and compressed. The second is that it utilizes an All-Reflective Interferometric Delay (ARID) method to introduce the finely controlled pulse delays. This method relies on angled stages (see figure S3) in order to create the coherence time delay with high accuracy and precision. Furthermore, this method elminates relative nonlinear dispersion introduced by previous glass wedge based methods.[3,4] This nonlinear dispersion can lead to distortions in two-dimensional spectra.[5,6]

In this implementation, continuum pulses were generated by focusing the output of a Ti:Sapphire oscillator seeded regenerative amplifier (4W, 5 kHz, 40 fs pulses centered at 800 nm) into 2 atmospheres of argon (f=1m). A dichroic mirror elminate the signal above 700nm. The pulse is compressed using Multiphoton Intrapulse Interference Phase Scan (MIIPS) as described in the text. We use 520-700nm pulses with 0.5% stability (std/mean measured at 10 Hz), which are compressed to 8-10fs. Figure S4 plots at typical transient grating and MIIPS autocorrelation trace. Beams 1 and 2 are seperated from beams 3 and 4, and 1 and 2 are delayed using a linear mounted retroreflector (Aerotech). Beam 4 is used as a local oscillator which co-propagates with the signal, and is set using a manual delays stage to be approximately 1 ps after the signal, and attennuated by an 3 orders of magnitude. We delay beam 1 relative to 2 using All-Reflective Interferometric Delay (ARID). In ARID, angled stages move nearly perpidcular to the direction of propagation of each beam (<0.5 degrees). This translates stage motion into very minimal delay of the beam, approximately 34 fs/mm of motion, compared to ~6660 fs/mm in other reflective implementations, at the cost of a small deviation from the BOXCAR geometry, which can be characterized using solvent transient grating. This deviation is characterized in a recently submitted manuscript.[7] Stages were calibrated using spectral interferometry. All four beams are put into a boxcar geometery with 1.2cm between each beam, and focused onto the sample with an 30 degree off-axis parabolic mirror (EFL: 45 cm), to a 100 micron spot size, which minimizes frequency-dependent directional filtering.[8] Photon flux was adjusted such that fewer than 0.3 excitations per QD are allowed, to ensure operation in the in the single exciton manifold (14 nJ/pulse and sample OD of 0.3 at 630 nm).[9,10] The signal and local oscillator is then focused onto a spectrometer and camera (Andor Shamrock and Newton respectively).

Data Processing

In figure S5, we show the data analysis procedure. We collect an interferogram for each coherence time ranging from -60 to 80 fs. We first Fourier interpolate from wavelength (collected on the camera) to frequency space (λ_t to ω_t), by zero padding the FT of the data by factor of 10, and using the expanded vector to linearly interpolate between points.[11] We then Fourier transform over ω_t to create a t vs τ plot, which we apodize in the t domain with a 300 fs window to eliminate scatter and homodyne components. The final 2D spectrum (ω_t vs ω_τ) is created by Fourier transforming over both domains, for example figure S7. We zero-pad by a factor of 2 in the ω_τ domain to better resolve features. The experiment was repeated several times (for example, figure S6), and solvent-only spectra were taken for comparison, contributing 10% of the signal at T=0, and negligible signal by T=10 fs.[12] To avoid non-resonant solvent signals, all analysis is performed for signals after the first 15 fs. Each individual spectrum is phased to separately collected broadband pump-broadband probe data (figure S5).[3] Spectrally resolved continuum-pump continuum-probe spectra were collected for each waiting time. The pump beam was modulated at 2.5 kHz, and pump-probe and probe-only spectra were collected on a high-speed line scan camera. TA spectra were acquired for all time delays corresponding to the waiting times of the 2D spectra. Applying the projection-slice theorem, we fit the projection of the real part of the 2D spectrum onto the ω_t axis to the TA spectrum.[13]

$$PP(T,\omega_t) = \mathrm{Re}\left\{ A \int_{-\infty}^{\infty} S_{2D}(\omega_\tau, T, \omega_t) \exp\left(i\phi + i(\omega_t - \omega_0)t_c + i(\omega_t - \omega_0)^2 t_q^2 + i(\omega_\tau - \omega_0)\tau_c d\tau \right) \right\} \quad (S1)$$

with ϕ_c, t_c, t_q, and τ_c are slight corrections to the measured timings and phase between each electric field.

TEM of QDs

a)

25
20
15
10
5

Size Distribution

1 2 3 4
Radius (nm)

20 nm

b)

XRD of QDs

Intensity

0.5

0

10 20 30 40 50 60 70 80
2θ (degrees)
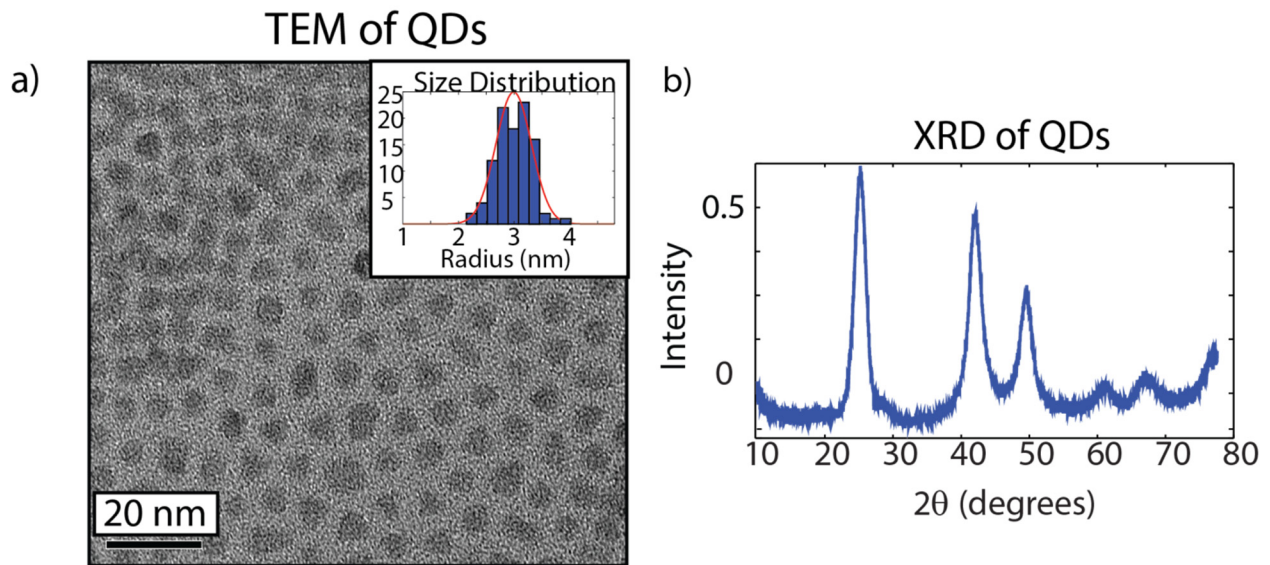
Figure S1: a) TEM image showing the QD ensemble used in this experiment r=3.0 ±0.3nm. The inset shows a histogram of particle sizes along with the estimate for the Gaussian distribution. b) XRD of the these particles showing zinc blende crystallinity.
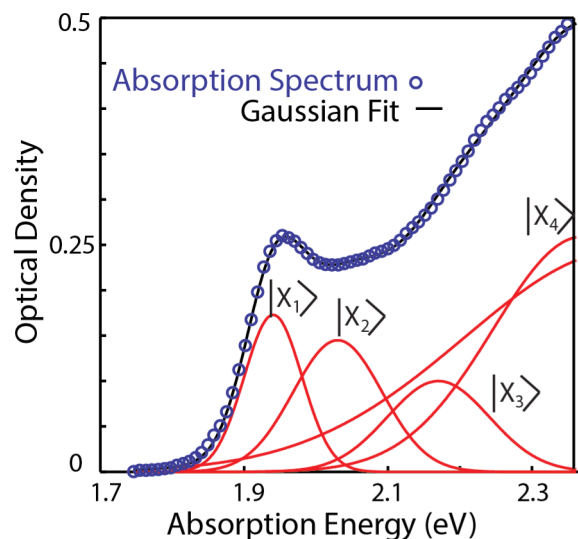

Figure S2: A fit of the absorption spectrum to a five Gaussian function. The first three peaks in the fit show good agreement to peaks from more monodisperse zinc-blende QD preparations. The other states are not clearly distinguishable from very broadband Gaussians, and thus we do not assign them with confidence.
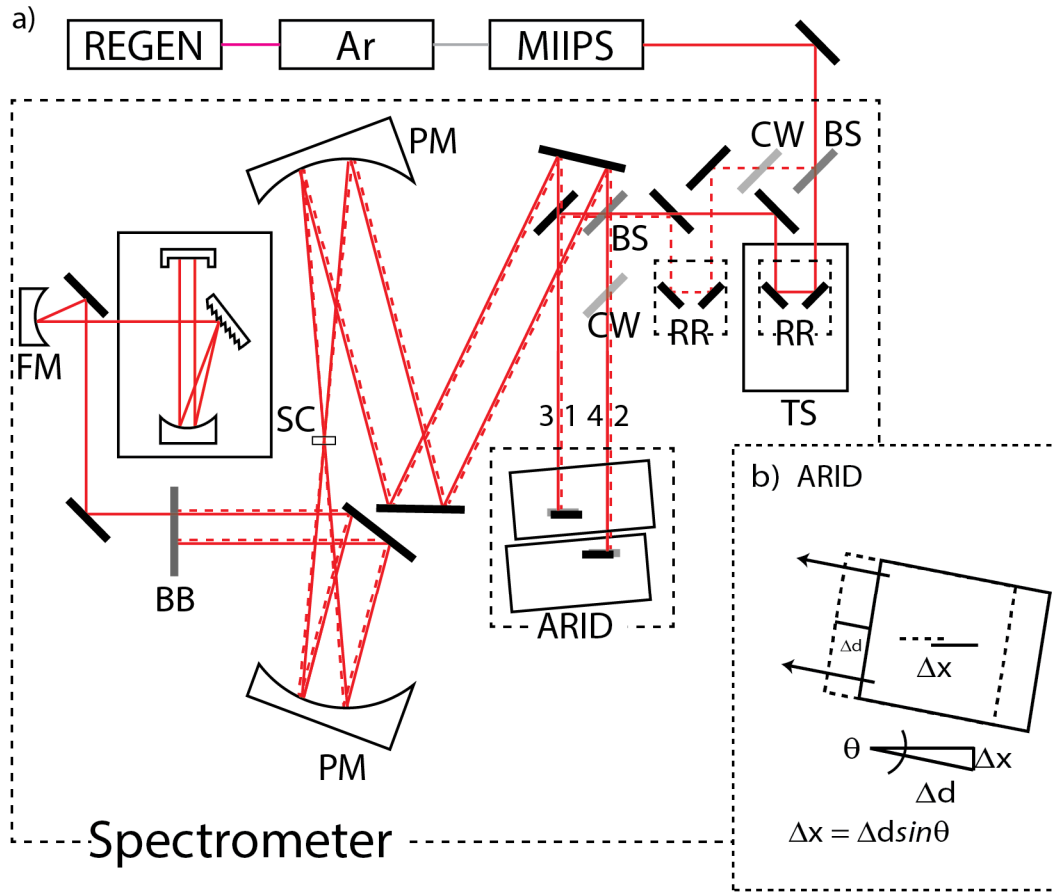
Figure S3: a) C-2DES setup. The details of this spectrometer and full characterization are the subject of a separate manuscript.[7] Broadband light is generated and compressed as described in the text. The beams are separated using beamsplitters (BS) and amount of glass in all beams is balanced with compensating windows (CW). We introduce a waiting time delay utilizing retroreflectors (RR) and a motorized translation stage (TS). All-Reflective Interferometric Delay (ARID) introduces the coherence time delay, and a 30 degree off axis parabolic mirror (PM) focuses the beams to a spot on the sample. All beams are blocked (BB) except the signal and the LO, which are focused on the spectrometer and camera (SC). b) ARID generates time delays by angling the direction of the stage motion nearly perpendicular (0.3°) to the direction of beam propagation. Therefore a distance Δd leads to a small change Δx in the forward direction of the mirror.
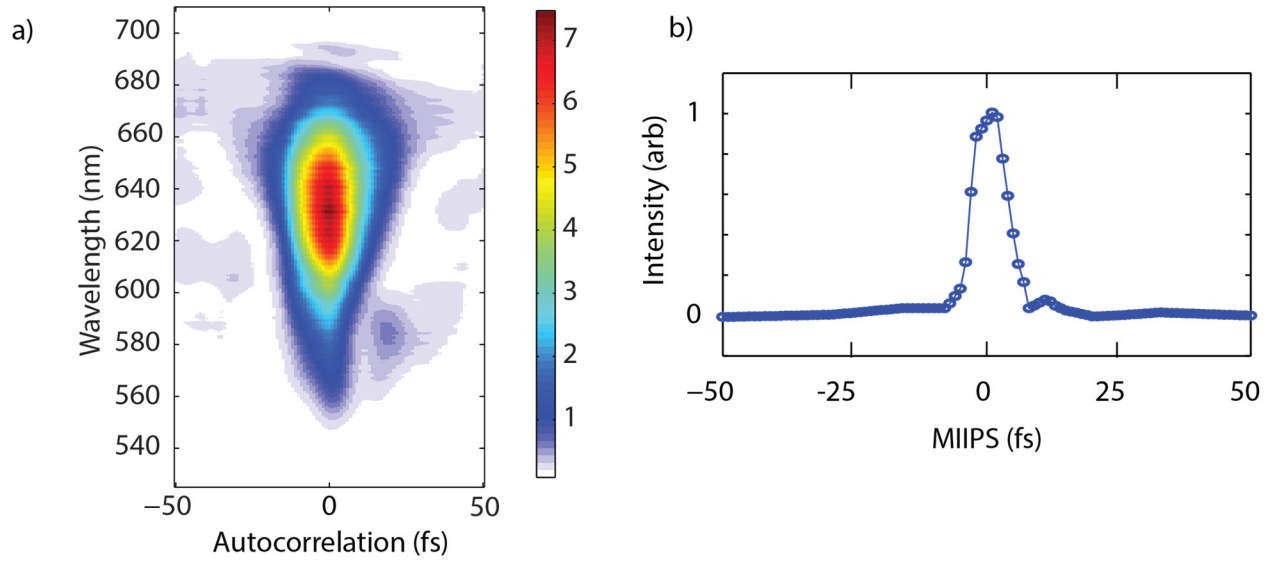
Figure S4: a) A typical TG-FROG trace, taken by overlapping beams 1 and 2 in time and scanning beam 3. The resultant TG signal is frequency resolved on the camera. A typical autocorrelation from this method measured ~ 10fs. b) A pulse duration measurement taken using the Multiphoton Intrapulse Interference Phase Scan (MIIPS) method displays a ~9 fs pulse.
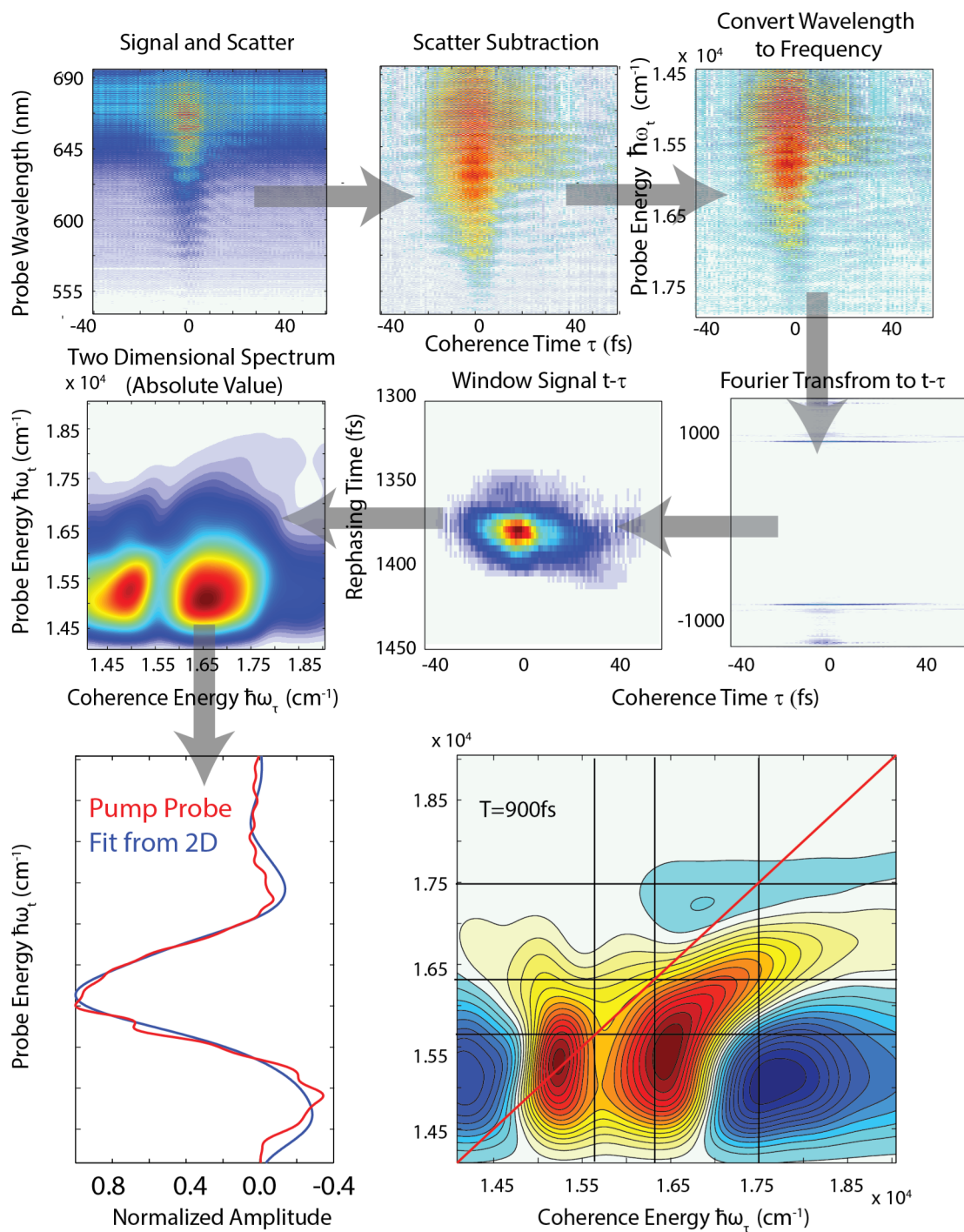
Figure S5: Representative spectra taken from a typical data analysis procedure. For every coherence time, τ, an interferogram is collected, which represents signal and scatter interfering with the local oscillator. Scatter is collected and subtracted for each coherence time, and the signal is Fourier transformed into t vs τ domain where it is apodized using a Hann window. For clarity, we display the magnitude of the signal in this domain. The t vs τ signal is Fourier transformed over both time domains to generate a magnitude ω_t vs. ω_t

spectrum. This spectrum is phased by fitting the summed down the real portion of the 2D spectrum to separately collected pump-probe according to equation S1.
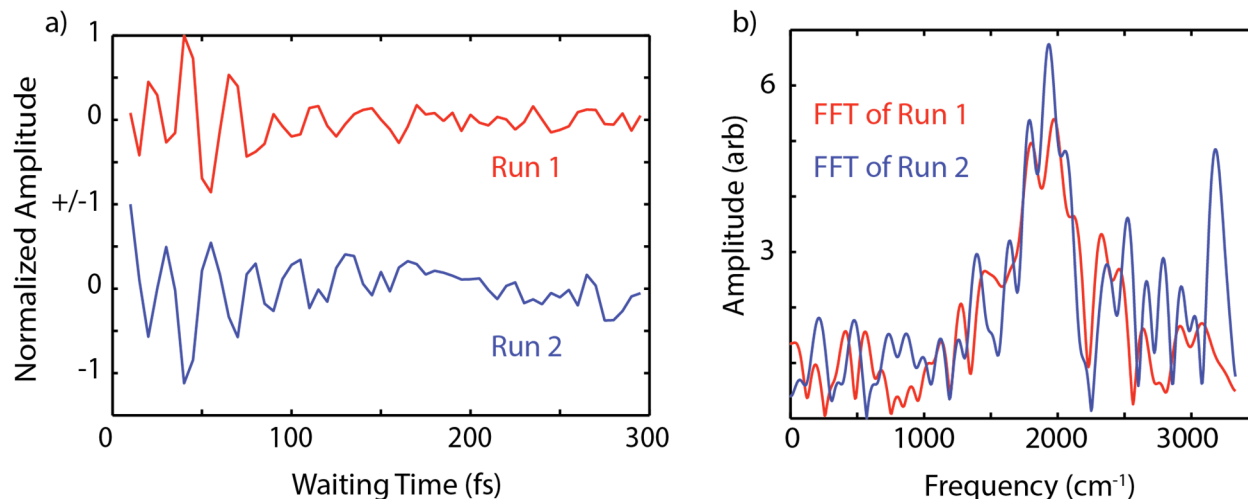

Figure S6: a) We demonstrate oscillation reproducibility from the same point in the 2D spectrum ($\hbar\omega_\tau$=2.17, $\hbar\omega_\tau$=2.05) taken from different days, with different pulse power and pulse compression conditions. The oscillations agree both in character, magnitude and frequency, but show different phase. The phase difference may be a result of small differences in compression (chirp). The pulse energies were 14 nJ/pulse for run 1 and 16 nJ/pulse for run 2.
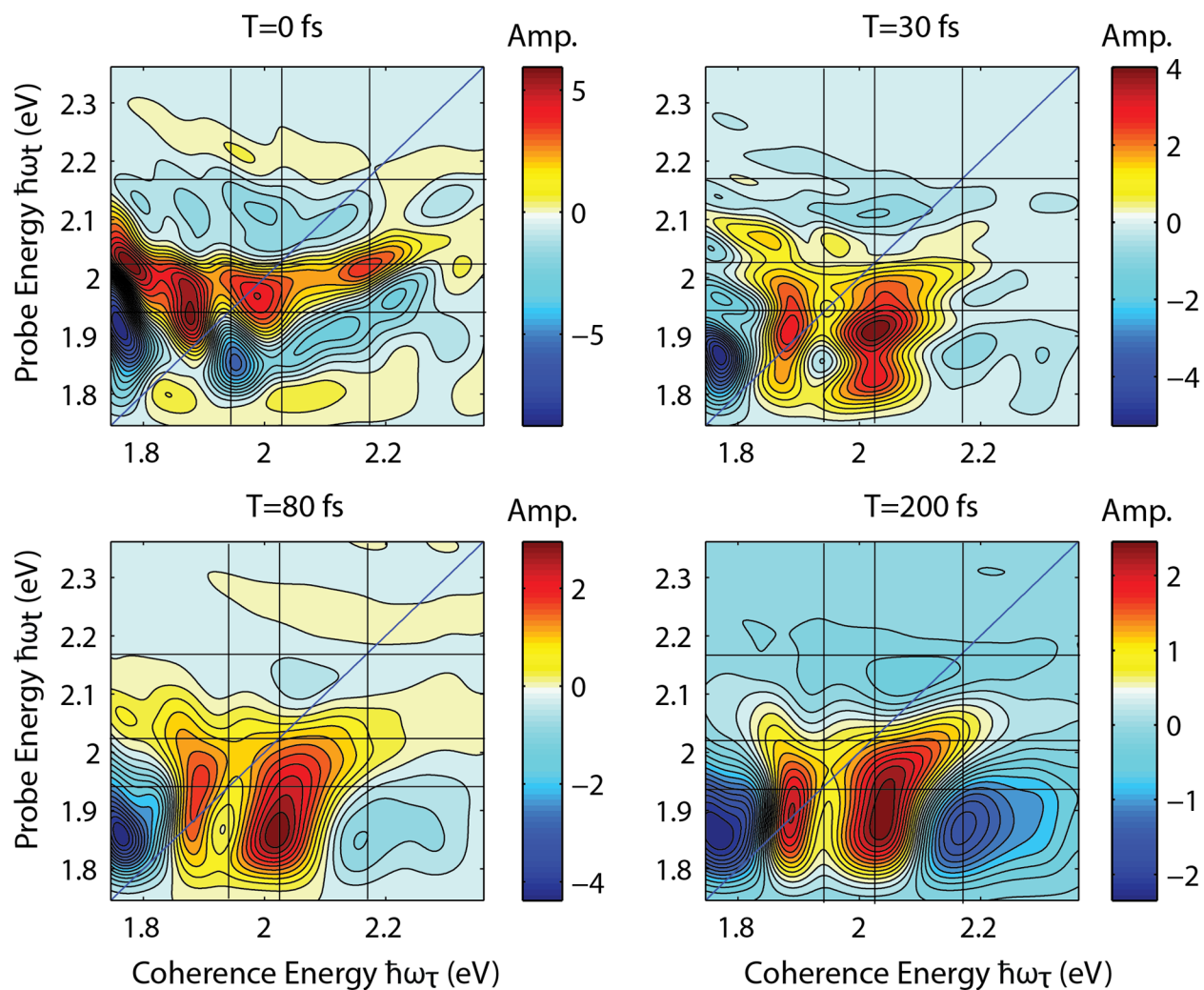
Figure S7: Four 2D spectra from different waiting times. The characteristics of the stimulated emission/ground state bleach signal between the 1P/1S states evident in the lower cross peak are the subject of a separate manuscript.[14]
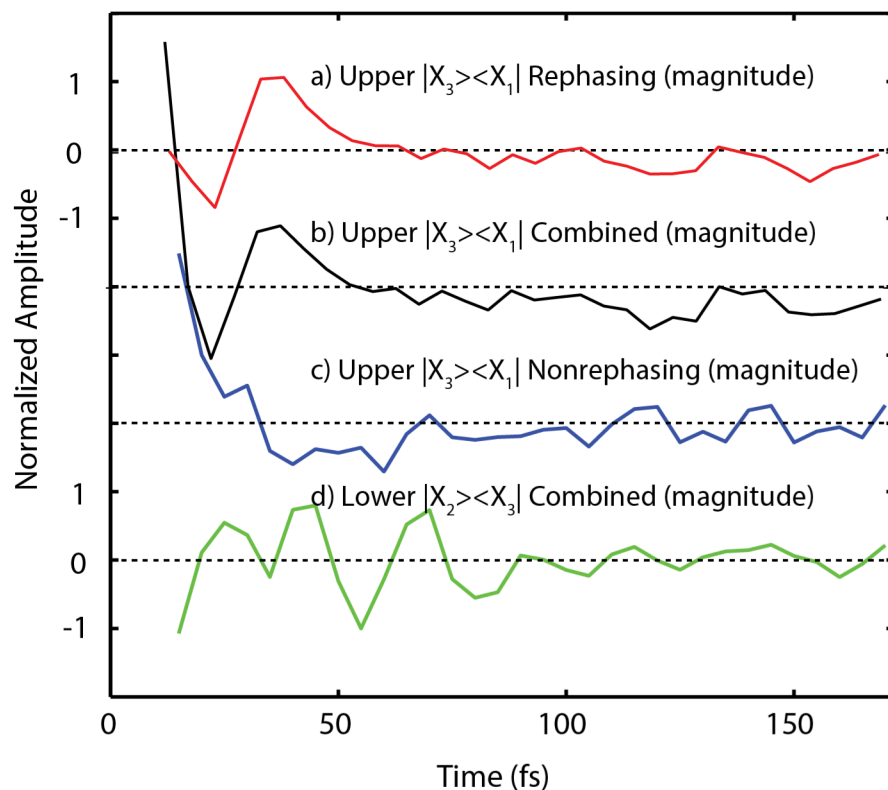
Figure S8: Traces taken from different regions of the spectrum. Trace (a-c) are taken from the magnitude of the upper diagonal cross peak between $|X_3\rangle$ and $|X_1\rangle$, while trace (d) is taken from the magnitude of the below diagonal $|X_3\rangle/|X_2\rangle$ peak. (a) Is extracted from the $\tau>0$ rephasing spectra while (b) and (d) are taken from the combined spectrum and (c) is taken from the $\tau<0$ nonrephasing spectrum. As can be seen both trace (a) and (b) show a high amplitude early time coherent oscillations, while (c) shows no clear early time coherent signature, consistent with the expectation for an electronic coherence. Trace (d) demonstrates that the magnitude taken from point **A** in the main text also shows clear oscillatory dynamics similar to those reported in the phased 2D spectra, indicating that the oscillations are not the result of phasing error.

References

1.   O. Chen, X. Chen, Y. Yang, J. Lynch, H. Wu, J. Zhuang, and Y.C. Cao, Angew. Chem. Int. Ed. **47**, 8638 (2008).
2.   D. Kartashov, S. Aliauskas, A. Puglys, A. Voronin, A. Zheltikov, M. Petrarca, P. Béjot, J. Kasparian, J.-P. Wolf, and A. Baltuka, Opt. Lett. **37**, 3456 (2012).
3.   T. Brixner, T. Mančal, I.V. Stiopkin, and G.R. Fleming, J. Chem. Phys. **121**, 4221 (2004).
4.   M.L. Cowan, J.P. Ogilvie, and R.J.D. Miller, Chem. Phys. Lett. **386**, 184 (2004).
5.   P.F. Tekavec, J.A. Myers, K.L.M. Lewis, F.D. Fuller, and J.P. Ogilvie, Opt. Express **18**, 11015 (2010).
6.   P.A. Tekavec, K.L.M. Lewis, F.D. Fuller, J.A. Myers, and J.P. Ogilvie, Selected Topics in Quantum Electronics, IEEE Journal of **18**, 210 (2012).

[7] H. Zheng, J.R. Caram, P.D. Dahlberg, B.S. Rolczynski, S. Viswanathan, D.S. Dolzhnikov, A. Khadivi, D.V. Talapin, and G.S. Engel, (submitted).

[8] M.K. Yetzbacher, N. Belabas, K.A. Kitney, and D.M. Jonas, J. Chem. Phys. **126**, 044511 (2007).

[9] E. Harel, S.M. Rupich, R.D. Schaller, D.V. Talapin, and G.S. Engel, Phys. Rev. B: Condens. Matter **86**, 075412 (2012).

[10] V.I. Klimov, J. Phys. Chem. B **104**, 6112 (2000).

[11] L. Lepetit, G. Chériaux, and M. Joffre, J. Opt. Soc. Am. B **12**, 2467 (1995).

[12] G.B. Griffin, S. Ithurria, D.S. Dolzhnikov, A. Linkin, D.V. Talapin, and G.S. Engel, J. Chem. Phys. **138**, 014705 (2013).

[13] T. Brixner, J. Stenger, H.M. Vaswani, M. Cho, R.E. Blankenship, and G.R. Fleming, Nature **434**, 625 (2005).

[14] J.R. Caram, H. Zheng, P.D. Dahlberg, B.S. Rolczynski, G.B. Griffin, D.S. Dolzhnikov, D.V. Talapin, and G.S. Engel, (submitted).